Composite Structures 141 (2016) 50–62

Contents lists available at ScienceDirect

Composite Structures

journal homepage: www.elsevier.com/locate/compstruct

Development of a physics-based multi-scale progressive damage model for assessing the durability of wind turbine blades

John Montesano [1], Hao Chu, Chandra Veer Singh *

Materials Science and Engineering, University of Toronto, 184 College St., Suite 140, Toronto M5S 3E4, Canada

ARTICLE INFO

Article history:
Available online 18 January 2016

Keywords:
Wind turbine blades
Multi-scale model
Computational micromechanics
Damage mechanics
Finite element analysis
Fatigue progressive failure

ABSTRACT

A physics-based multi-scale progressive damage model was developed for predicting the durability of wind turbine blade structures. Computational micromechanics was coupled within a continuum damage mechanics (CDM) framework, and implemented through a user-defined subroutine within commercial finite element software, for evaluating sub-critical damage evolution and stiffness degradation of the blade structure. The study is the first step in developing an accurate prediction model for composite wind turbines that accounts for the multi-scale nature of damage in rotor blades. The quasi-static and fatigue simulation results demonstrate the ability of the model to predict the evolution of damage in the critical regions of the blade structure, which is an important contribution and essential for increasing the accuracy of damage tolerance analyses and for certification of composite structures. A parametric study of blade geometric parameters also revealed a correlation with damage evolution, providing valuable insight for optimization of blade designs.

© 2016 Elsevier Ltd. All rights reserved.

1. Introduction

As the global need for renewable energy expands, designing wind turbines with greater power harnessing capacity is paramount. One solution is to increase the rotating blade length, however, this raises the demands on the blade structure since its weight, and thus gravitational load, also increases. Therefore, minimization of blade weight becomes an even more important design requirement. When in service, composite wind turbine blades must resist damage caused by extreme wind gusts as well as cyclic external loading [1]. As the blades rotate during operation, changing aerodynamic and gravitational loads give rise to cyclic bending in the flap-wise and edge-wise directions (see Fig. 1a), which causes damage to evolve and the stiffness to degrade. Since wind turbines are expected to last 20–30 years in service, the fatigue requirements for blade designs are quite high. Despite composite materials having excellent fatigue properties, progression of damage during service is one of the main limiting factors for increasing rotor blade length. Since the evolution of fatigue damage in composite materials currently used for rotor blades is not well understood, large safety factors are employed which lead to highly conservative designs. With a better understanding of the damage evolution characteristics of rotor blade structures, it will be possible to decrease these safety factors and optimize designs by tailoring the laminate stacking sequences and through parametric studies, thereby reducing service life costs. Thus, there is a need to develop comprehensive modeling tools for predicting progressive failure of composite wind turbine blades (i.e., damage tolerance analysis) if larger wind turbine structures are to be improved and certified. Specifically, we need to develop multi-scale models that consider the different length scales at which different damage modes are observed to nucleate and progress [2].

Only a few studies have investigated damage and failure modes of full-scale wind turbine blades [3–6]. In the report by Sorensen et al. [3], examination of fully collapsed rotor blades revealed that the main damage modes were spar cap-skin and upper–lower skin joint adhesive debonding, sandwich panel face-core debonding, laminate delamination, and blade local buckling (see Fig. 1a). They also indicate that laminate delamination was present in the regions containing many ply cracks. Other studies observed that ply delamination was the main damage mode that initiated structural collapse of the blades [4,6]. These studies all focus on the structural collapse of rotor blades and the associated damage modes at the macroscopic scale, whereas microscopic damage modes are not discussed at great length. The studies by Lambert et al. [7] and Sorensen [1] reveal that a high density of matrix

* Corresponding author. Tel.: +1 (416) 946 5211; fax. +1 (416) 978 4155.
E-mail addresses: john.montesano@uwaterloo.ca (J. Montesano), hao.chu@mail.utoronto.ca (H. Chu), chandraveer.singh@utoronto.ca (C.V. Singh).
[1] Present address: Mechanical and Mechatronics Engineering, University of Waterloo, 200 University Ave. West, Waterloo N2L 3G1, Canada.

http://dx.doi.org/10.1016/j.compstruct.2016.01.011
0263-8223/© 2016 Elsevier Ltd. All rights reserved.

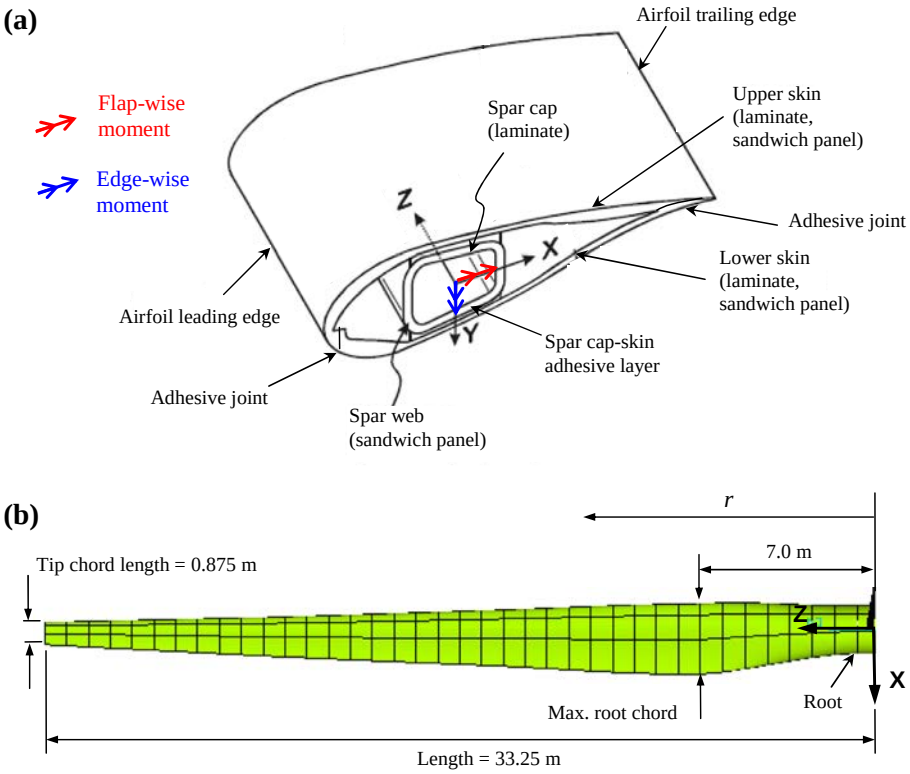

Fig. 1. (a) Schematic of typical two-spar wind turbine blade with structural details and (b) geometry of two-spar blade analyzed in this study.

cracks is a precursor to more critical damage modes such as delamination, but there is no comprehensive effort to quantify the effects of these microscopic cracks. It is clear that microscopic laminate ply cracks will accumulate and lead to the onset of critical damage modes, which will initiate structural failure modes such as adhesive joint debonding and local buckling.

A number of recent studies have reported computational models that analyze catastrophic failure in wind turbine blades subjected to quasi-static or cyclic loads [4,8–18]. Certain models do not explicitly consider damage evolution in wind turbine blades [9,15], while others only consider damage evolution in the materials used to manufacture wind turbine structures [13,16,18]. In addition, although some models simulate damage evolution in rotor blades, they often utilize failure criteria such as Hashin's or Puck's criteria without accounting for any physical damage modes or the corresponding material stiffness degradation [10,12,14], which must be considered in order to accurately capture the nonlinear behavior of the materials used in the analysis of these structures and for service life prediction. Failure criteria lack any physical basis and do not properly consider the ply constraining effects in laminates, which was clearly illustrated in a recent article by Talreja [19]. For studies that consider fatigue damage evolution, simple damage models based on stress-life (S-N) test data or non-physical macroscopic variables are often used [10,11,17], providing limited confidence in these approaches. In general, most models reported in the literature rely on extensive test data for damage model calibration, which requires complicated and costly experimental programs every time there are structural design changes. This is regarded by the authors as a major drawback since the predictive capabilities of existing approaches are limited in scope and application. Furthermore, the reported wind turbine rotor blade progressive failure models predominately account only for the macroscopic damage modes and the ensuing structural collapse [4,8], without considering the progressive nature of sub-critical microscopic intra-laminar damage, which is imperative for predicting onset of macroscopic failure modes. Thus, consideration of the multi-scale nature of progressive damage in wind turbine blades is vital for accurate long-term durability assessment.

Based on the above considerations, the multi-scale nature of damage evolution in composite structures has attracted significant attention in recent years, leading to the development of useful multi-scale approaches whereby the evolution of sub-critical damage modes has been accounted for [20–28]. For instance, Bogdanor et al. [20] developed a new probabilistic multi-scale model that accounted for the stochastic nature of failure in composite laminates. In this model, the variability of the constituent material properties at the microscopic length scale is linked to the laminate length scale using a reduced-order computational homogenization model, and predictions for the tensile strength variability of open hole multidirectional laminated plates has been reported. Ply-level failure data from unidirectional laminate experiments were used to calibrate the computational model, however, in-situ ply strengths were not considered in the study. Camanho and co-workers [24], on the other hand, have developed a model that considers the evolution of intra-ply damage (i.e., ply cracking) as well as delamination growth for multidirectional laminates. Micromechanics within a continuum framework was used to address the energetics of ply cracking, where damage evolution laws for both tensile and compressive loading follow mathematical functions that utilized experimentally-derived fracture toughness values. In addition, a bilinear cohesive damage model was used to account for delamination and was implemented into a finite element (FE) model using cohesive elements. The intra-ply damage model was also implemented into a commercial FE package and foreign impact damage progression in flat composite plates was simulated. Following a continuum damage mechanics based approach, Waas and co-workers [26] have developed a multi-scale model for multidirectional laminates in which the microscopic damage evolution

and eventual failure are considered separately at their respective characteristic length scales by utilizing distinct internal variables. This physics-based model was implemented into a commercial FE package in order to simulate damage evolution in various notched plate geometries under quasi-static loading, where a smeared crack approach was used to ensure mesh size objectivity. Finally, Wisnom and co-workers [27,28] recently studied damage evolution of notched multidirectional laminated plates under axial quasi-static loading, and developed a FE model that explicitly simulates intra-ply cracking and delamination using cohesive elements. The model is unique in the sense that it also accounts for fiber fracture using a failure criterion based on Weibull statistics along with a corresponding element deletion technique. Overall, these cited studies have made notable contributions towards developing physically-based simulation models for predicting damage evolution in composite structures. Nonetheless, accurate prediction of deformational behavior of multidirectional laminated composite structures undergoing progressive damage under multiaxial loading still remains a big challenge.

The aim of this study is to develop a practical multi-scale model for predicting damage evolution and stiffness degradation in long composite wind turbine blades manufactured with multidirectional laminates, while providing a balance between accuracy and computational efficiency. One of the main modeling objectives is to utilize a multi-scale modeling philosophy in order to reduce, not eliminate, the number of experimental tests required to calibrate the material damage parameters. In recent work, the authors developed a synergistic damage mechanics (SDM) based model for predicting sub-critical microscopic damage evolution in multiaxially loaded laminates [29,30], which will be the basis for the model developed here. This work is the first step in developing a simulation model that can accurately predict the multi-scale nature of progressive failure in wind turbine blade structures, which is required for damage tolerance analysis and, thus, for certification purposes. The developed simulation methodology includes a procedure for generating the blade geometry and applying external loads, which utilizes a multi-scale user-defined subroutine implemented into a commercial finite element (FE) software package and an algorithm that simulates quasi-static and cycle-by-cycle fatigue loading. Furthermore, a parametric study is presented in order to investigate the effects of blade geometry parameters on microscopic damage evolution, which is important for optimization of rotor blade designs.

2. Rotor blade details

A 1.5 MW horizontal axis wind turbine with 70 m rotor diameter was considered, which consists of three long two-spar rotor blades with blade length, tip chord and reference root chord of 33.25 m, 0.875 m, and 2.8 m, respectively (see Fig. 1). The open-source tool NuMAD [31] was used to generate the three-dimensional blade geometry. The rotor blade contained the same airfoil section along its length, namely the familiar NREL S818 airfoil [32], to simplify aerodynamic calculations. The tip airfoil section has no twist since it is parallel to the pitch angle, and the plunging airfoil leading edge ensures twist along the transitioning blade length towards the root as shown in Fig. 2. In this study, the pitch angle at the blade tip was assumed to be constant at 45°. At the root the blade transitions from a NREL S818 airfoil to a circular section with a 1.89 m diameter over the span of 7.0 m (see Fig. 1b). For the aforementioned parametric study, the twist angle was varied between 5° and 15° and the root (maximum) chord length was varied between 2.8 m and 4.8 m.

2.1. Blade loading

The main sources of loading on rotor blades during standard operational conditions are aerodynamic, gravitational and centrifugal loads. Other operational loads resulting from pitching and yawing of the blades, braking, or emergency stop scenarios are typically less intensive than gravitational loads [33], thus they were not considered in this work.

Aerodynamic lift and drag forces depend on the horizontal wind speed, v_w, blade tangential speed, $v_b(r)$, the airfoil twist, and the blade pitch angle, and are the major contributors to blade bending. The local angle of attack, α_w, is the angle between the resultant

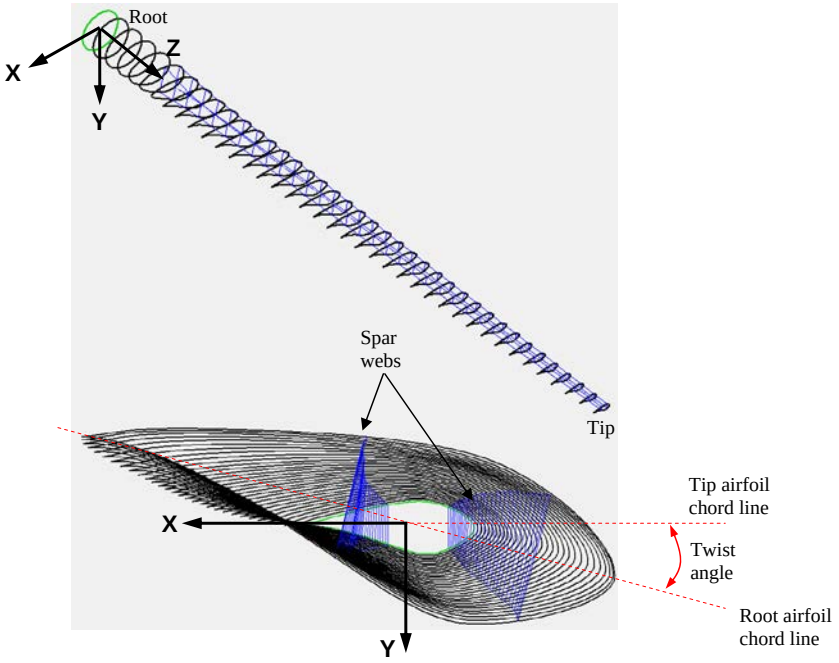

Fig. 2. Airfoil sections along the length of a rotor blade generated using NuMAD [31], showing the taper and twist of the blade as well as the spar webs.

wind speed, v_{res}, and the chord line, which is also a function of the local twist angle and the blade pitch angle (see Fig. 3). The resulting lift and drag forces act to bend the rotor blade in both the flap-wise and edge-wise directions as shown in Fig. 3. In this study the widely used blade element momentum (BEM) theory [12,15] was employed to evaluate the lift and drag force distribution at 15 discrete segments along the length of the rotor blade. The tip speed ratio, *TSR*, was assumed to be 7.0 since this is a common value for modern three-blade wind turbines [34]. For a given wind speed, v_w, the tip speed ratio was used to evaluate the blade rotational speed, ω, using:

$$TSR = \frac{\omega R}{v_w} \tag{1}$$

where R is the blade radius and $v_b = r\omega$. With the blade tangential speed distribution along the length defined, the α_w distribution was evaluated using the blade twist (see Fig. 2). The segment lift and drag forces were then evaluated using:

$$F_L = \frac{1}{2}\rho A C_L v_{res}^2 \tag{2}$$

$$F_D = \frac{1}{2}\rho A C_D v_{res}^2 \tag{3}$$

where $\rho = 1.225$ kg/m^3 is the air density and A is the planform area of the blade segment. The lift and drag coefficients, respectively C_L and C_D, are functions of local α_w, and were extracted from available NREL S818 airfoil data.

The mass-dependent gravitational and centrifugal loads were treated independently from the aerodynamic loads. Centrifugal forces resulting from rotation act radially outward along the blade axis, and are defined by:

$$F_C = m_{b,i}\omega^2 r \tag{4}$$

Here, $m_{b,i}$ is blade segment mass and r is distance of the segment from rotation center. The gravitational forces acting on blade segments are proportional to their mass. Their direction depends on the blade orientation, which will in fact continuously change during rotation. In this study, we assumed that the gravitational loads act along the direction shown in Fig. 3 in order to increase the effective load causing flap-wise bending (i.e., a worst-case scenario).

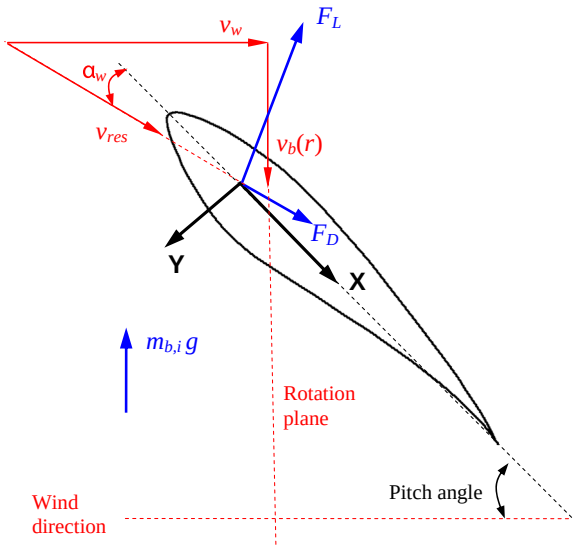

Fig. 3. Velocities and resulting aerodynamic forces on an airfoil section of a rotor blade at a distance r from the root.

Table 1
GFRP 0.5 mm thick ply in-plane elastic properties.

E_1 (GPa)	E_2 (GPa)	G_{12} (GPa)	ν_{12}
46	13	5	0.30

Table 2
Virgin GFPR laminate elastic properties from CLT.

Laminate	E_x^o (GPa)	E_y^o (GPa)	G_{xy}^o (GPa)	ν_{xy}^o	G_{xz}^o (GPa)	G_{yz}^o (GPa)
$[0/90/\mp 45]_s$	23.72	23.72	9.07	0.3079	4.1	4.1

2.2. Blade material

Wind turbine blades typically utilize many distinct laminate materials and sandwich panels to manufacture the skin and spar structures as shown in Fig. 1a. In order to simplify the blade model, it was assumed that the blade skins and spar webs/caps were manufactured from the same multidirectional $[0/90/\mp\theta]_s$ GFRP laminate. This laminate sequence was chosen to showcase the developed model capability for multi-mode damage scenario; however, the same model can easily be applied to other laminates. The properties of the 0.5 mm thick unidirectional plies are presented in Table 1, which have a corresponding density of 1800 kg/m^3. The in-plane laminate properties evaluated using classical laminate theory (CLT) are listed in Table 2, which also includes the out-of-plane shear moduli, G_{xz} and G_{yz}, evaluated using expressions reported by Davalos et al. [35].

3. Multi-scale damage model

In order to predict the durability of wind turbine blades, a new physics-based three-scale modeling approach illustrated in Fig. 4 was developed. The computational micromechanics component was used to evaluate ply crack surface displacements, and the laminate constitutive equations were developed within a continuum damage mechanics (CDM) framework for evaluating the laminate stiffness. The structural module required further model development for implementation of constitutive equations into FE software ANSYS via a user-defined subroutine (USERMAT), which was used to simulate progressive failure of wind turbine blade structures. Details of this hierarchical multi-scale modeling approach and the overall simulation procedure are discussed subsequently.

3.1. Micromechanics and laminate constitutive equations

The evolution of sub-critical microscopic ply cracks in multidirectional laminates subjected to general loading conditions is well documented [30,36–38]. Under static or cyclic loads ply cracks initiate and evolve in multiple plies (see Fig. 5), whereby a complex three-dimensional stress state ensues as a result of crack interactions influencing the ply constraining effects. The progressive nature of damage leads to degradation of the laminate stiffness, which may lead to a decline in their overall performance. The multi-scale model combines the SDM approach at the micro- and macro-scale with an energy based damage evolution model to capture these effects.

Assuming that microscopic ply cracks in a given ply of arbitrary orientation are uniformly spaced, self-similar and fully developed through the lamina thickness, then following a typical damage mechanics approach, the damage state for damage mode α (see Fig. 5) can be characterized through a second-order tensor as [39]:

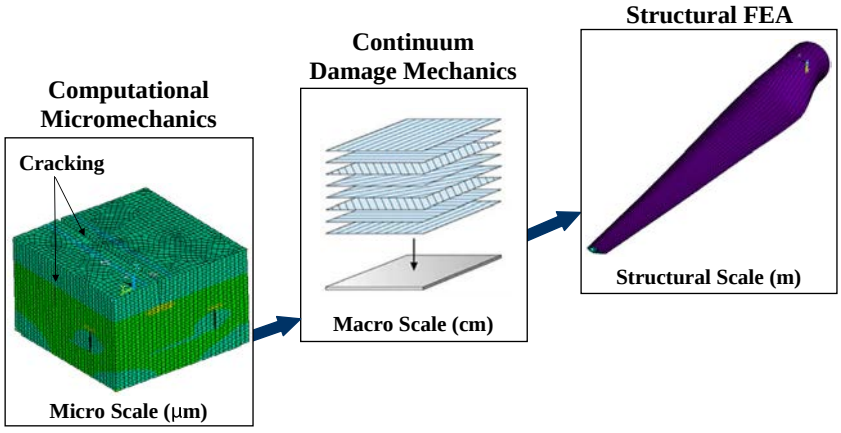

Fig. 4. Schematic of physics-based hierarchical synergistic multi-scale modeling approach.

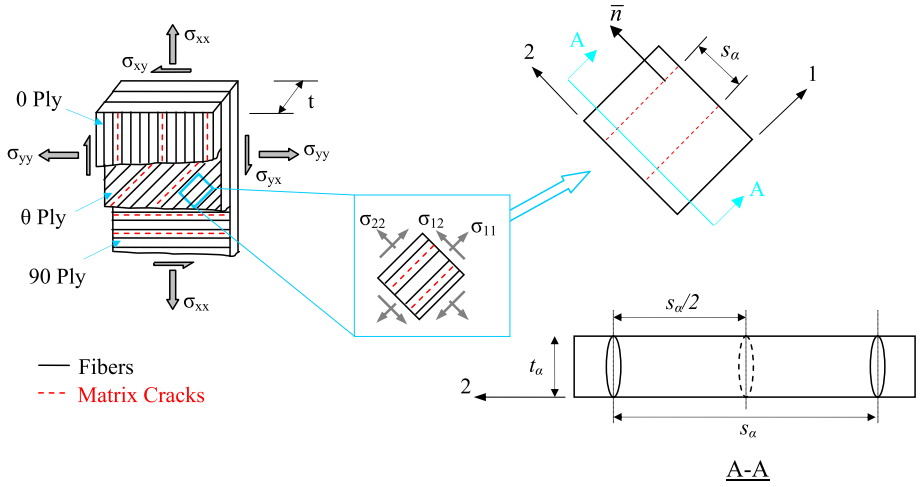

Fig. 5. Schematic of a cracked multidirectional laminate subjected to multiaxial loads, where local transformed stress components and crack spacing for a damage mode α are also shown.

$$D_{ij}^{(\alpha)} = \frac{\kappa_\alpha t_\alpha^2}{s_\alpha t} n_i n_j \tag{5}$$

Here, t_α, s_α, t, n_i $(i = 1,2,3)$ are the cracked ply thickness, average crack spacing, total laminate thickness, and crack surface normal unit vector components, respectively. The constraint parameter κ_α represents the corresponding ply constraining effect, and is a function of the crack opening displacements (COD). For thin symmetric orthotropic laminates containing damage, the Helmholtz free energy is formulated in terms of applied strain and damage tensor components, $\psi\left(\varepsilon_{ij}, D_{ij}^{(\alpha)}\right)$. Thereafter following the clausius–Duhem inequality, the overall stress–strain relationships in terms of the resultant stress tensor, σ_{ij}, are derived as:

$$\sigma_{ij} = C_{ijkl}\left(D_{ij}^{(\alpha)}(\rho)\right)\varepsilon_{kl} \tag{6}$$

where the stiffness tensor for a given crack density ρ is defined by:

$$C_{ijkl} = \frac{\partial^2 \psi}{\partial \varepsilon_{ij} \partial \varepsilon_{kl}} = \begin{bmatrix} \frac{E_x^o}{1-\nu_{xy}^o \nu_{yx}^o} & \frac{\nu_{xy}^o E_y^o}{1-\nu_{xy}^o \nu_{yx}^o} & 0 \\ \frac{\nu_{xy}^o E_y^o}{1-\nu_{xy}^o \nu_{yx}^o} & \frac{E_y^o}{1-\nu_{xy}^o \nu_{yx}^o} & 0 \\ 0 & 0 & G_{xy}^o \end{bmatrix} - \sum_\alpha a_\alpha D_\alpha \begin{bmatrix} 2a_1^{(\alpha)} & a_4^{(\alpha)} & 0 \\ a_4^{(\alpha)} & 2a_2^{(\alpha)} & 0 \\ 0 & 0 & 2a_3^{(\alpha)} \end{bmatrix} \tag{7}$$

The first term on the right hand side of Eq. (7) contains the undamaged orthotropic laminate engineering constants, and the second term represents stiffness changes brought about by damage in different modes. Here, $a_i^{(\alpha)}$ and D_α are respectively the orthotropic damage constants and the effective damage parameters for all damage modes of the laminate. Eq. (7) is valid for any general symmetric laminate under in-plane multiaxial loading, and is conducive for implementation into FE software, so long as all constraint parameters (κ_α) and damage constants $(a_i^{(\alpha)})$ are evaluated.

In lieu of costly experimental data, the κ_α and $a_i^{(\alpha)}$ terms were evaluated using three-dimensional micromechanical FE models that account for ply constraining effects, as well as intra-ply and inter-ply crack interactions [29]. Representative volume elements (RVE) of the crack-containing laminates were represented in the computational model using transversely orthotropic ply properties, and were meshed using 3D continuum elements. Cracks spanning the ply thicknesses were explicitly included in the 3D FE micromechanical model, where various crack scenarios were assessed. Periodic boundary conditions applied to the RVE allowed for proper representation of the laminate shear response under multiaxial loading. The κ_α parameters were defined using computationally evaluated crack surface displacements averaged from the nodal displacements at the crack surfaces. The $a_i^{(\alpha)}$ terms were evaluated by using the volume averaged stresses and strain, along with Eq. (7). Note, in the analysis it was assumed that the cracks in each ply span the ply thickness and have uniform spacing, however, the crack spacing in adjacent plies can be independent.

Experimental evidence suggests that ply crack spacing is not uniform at lower crack densities, but tends to be uniform at higher crack densities [40]. In order to test the model accuracy, computationally predicted stiffness degradation data for various damage scenarios were compared to available experimental data in Ref. [29]. An excellent correlation was found, which demonstrated that the model parameters are correctly bounded. It should also be noted that although the out-of-plane laminate moduli, G_{xz} and G_{yz}, were required, their degradation was assumed to have negligible effect on in-plane moduli [41].

To predict ply crack density evolution, an energy approach based on linear elastic fracture mechanics concepts was developed. Consider two cracks states for an arbitrarily oriented ply in a laminate caused by an increasing applied load, with crack spacings denoted by s_α and $s_\alpha/2$ (see Fig. 5). If energy associated with mode I and mode II is considered, the work required to close the new cracks in opening and sliding directions is defined by [30,42]:

$$W_I = \frac{(\sigma_2^\alpha)^2 t_\alpha}{E_2}\left[2\tilde{u}_n^\alpha(s_\alpha/2) - \tilde{u}_n^\alpha(s_\alpha)\right],$$
$$W_{II} = \frac{(\sigma_{12}^\alpha)^2 t_\alpha}{E_2}\left[2\tilde{u}_t^\alpha(s_\alpha/2) - \tilde{u}_t^\alpha(s_\alpha)\right] \quad (8)$$

Here, E_2 is the transverse modulus of the undamaged ply, σ_2^α is the transformed ply level stress acting normal to the crack plane evaluated using CLT, σ_{12}^α is the corresponding stress acting tangential to the crack plane, $\tilde{u}_n^\alpha$ and $\tilde{u}_t^\alpha$ respectively denote the averaged CODs normalized with respect to the ply thickness, and normalized average crack sliding displacements (CSDs) associated with a specific damage mode. For any given loading condition, the criterion for ply crack initiation or multiplication is based on the following relation:

$$\left(\frac{W_I}{G_{Ic}}\right) + \left(\frac{W_{II}}{G_{IIc}}\right)^2 \geqslant 1 \quad (9)$$

The ply-dependent critical energy release rates associated with mode I and mode II are denoted by G_{Ic} and G_{IIc}, respectively, and are typically defined by fitting mathematical models to experimental data. In this study, these parameters were evaluated for each ply in a laminate using a numerical approach based on a modified crack tip closure technique. Note that the computationally evaluated G_{Ic} and G_{IIc} do account for the corresponding ply constraining effects, and thus Eq. (9) can be used to evaluate the in-situ ply crack initiation strains. It is also worth noting that a virtual crack technique is used to determine the initiation and evolution of ply level cracks, where a finite number of segments (or links) in each ply are considered for the cracking process. Note that the damage progression criterion in Eq. (9) does not require experimental inputs and has been previously validated with independent experimental data in Ref. [30].

In addition, the stochastic nature of the ply crack multiplication process, which results from a random distribution of manufacturing flaws, local fiber fractions, or weakened fiber matrix interfaces, was accounted for through a two-parameter Weibull distribution of G_{Ic} and G_{IIc}. As an example for mode I cracking, the energy release rate is defined by:

$$G_{Ic} = G_o\left[\ln\left(\frac{1}{1-F}\right)\right]^{\frac{1}{m}} \quad (10)$$

where G_o and m are the Weibull distribution parameters, and F is a random number in the interval [0,1]. The two Weibull parameters were evaluated from the mean and variance of G_{Ic}, where the mean value is defined numerically as indicated above and the standard deviation is assumed to be 10% (i.e., a scatter of ±10%). A similar distribution was utilized for G_{IIc}. Recent studies by Bazant and coworkers [43,44] have established that for quasi-brittle and brittle materials, a Weibull distribution is not completely physically justified due to the inherent assumptions of infinite links in the chain underlying the weakest-link model. It is noted that the current model does not suffer from this limitation as we begin the cracking simulations with a finite number of links [30].

The critical energy release rates defined above are suitable for quasi-static conditions where W_I and W_{II} tend to continuously increase as a result of increasing ply stresses. For constant amplitude cyclic loading with constant W_I and W_{II} values (see Eq. (8)), the defined G_{Ic} and G_{IIc} values will not allow for multiplication of ply cracks. Note that as the ply crack density increases, the intra-ply crack shielding effect will in fact lead to decreasing crack displacements, and thus decreasing W_I and W_{II} values. As a result, it can be inferred that the observed ply crack density evolution during constant amplitude cyclic loading of laminates is a result of decreasing energy thresholds (i.e., G_{Ic} and G_{IIc}). Experimental data shows that the ply crack density evolution for laminates under fatigue increases rapidly during the early stages and eventually reaching a saturation state [45], which suggests that the energy thresholds must follow a similar, but inverse, trend during this stage of cycling. Here, we propose a new approach where the rates of change of G_{Ic} and G_{IIc} are defined through an analytical model that relates to the number of loading cycles, n. As an example, for CODs of ply cracks under arbitrary applied loading, the rate of change of G_{Ic} is given by:

$$\frac{dG_{Ic}}{dn} = cG_{Ic,o}n^{c-1} \quad (11)$$

Here, $G_{Ic,o}$ is the stochastic ply critical energy release rate evaluated using Eq. (10), and c is a ply-level constant that was evaluated by considering the experimental data reported by Tong et al. [36] for the same GFRP laminate considered.

3.2. Structural scale

In order to simulate sub-critical damage evolution in wind turbine blades, the model developed in Section 3.1 was extended to include a structural module, where the laminate constitutive equations were implemented into ANSYS through a Fortran-based USERMAT [46]. The form of the constitutive law (i.e., Eqs. (5)–(9)) allows for direct use with displacement-based elements; however, this implementation was not a trivial task since multiple algorithms were developed in order to control the subroutine iterative solutions as well as the overall simulation, as will be discussed hereafter. The USERMAT flowchart is shown within the diagram of Fig. 6, which highlights the developed iterative energy-based crack multiplication technique, the corresponding stiffness degradation algorithm and the computational micromechanical component. When the subroutine was engaged, the crack multiplication algorithm iterated to determine the degree of crack multiplication within a ply for the current load step or cycle using the criterion defined by Eq. (9), which was repeated for all plies in the laminate until the solution converged. Once the current laminate damage state was defined, the corresponding stiffness and stress tensors were evaluated using Eqs. (7) and (6), respectively, and passed back to ANSYS. During these iterations, the micromechanical component provided the required input for the crack multiplication scheme and for evaluation of the degrading stiffness tensor (see Fig. 6).

One of the challenges in creating the structural module was integrating NuMAD within the simulation environment for generating the blade geometry. This was accomplished through ANSYS APDL based algorithms, and meshing of the blade skin panels and spars was performed using higher-order 8-node SHELL281 elements with orthotropic material properties listed in Table 2.

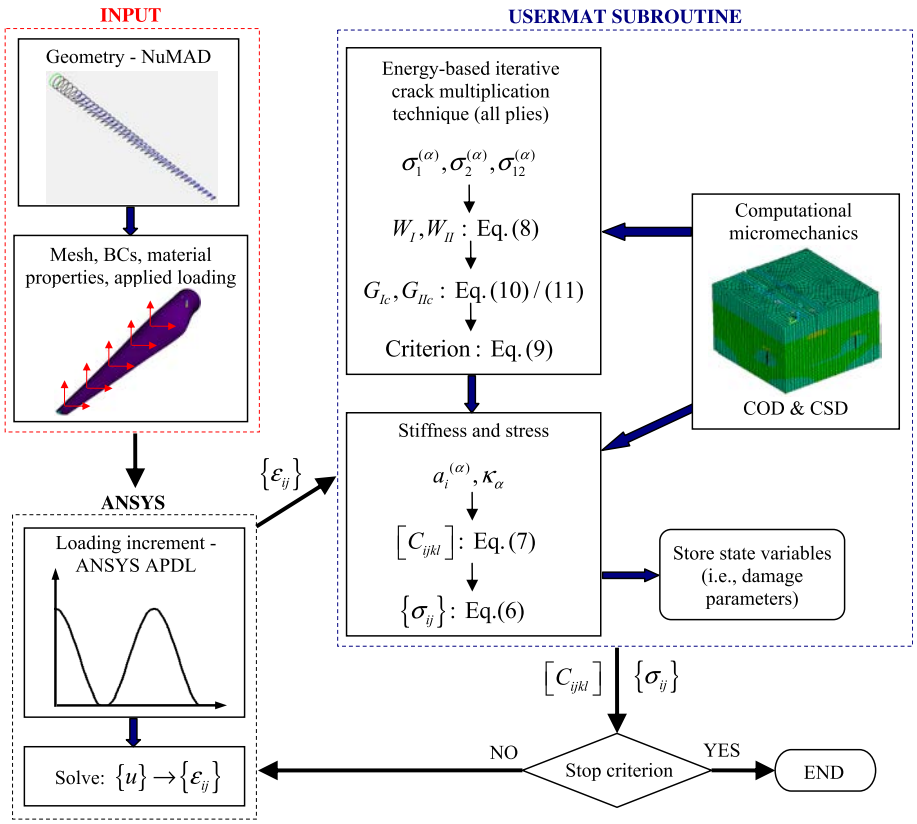

Fig. 6. Simulation package flowchart highlighting implemented multi-scale model.

It should be noted that the element size was kept larger than the RVE defined for the micromechanical component, which was necessary in order to ensure applicability of the constitutive equations since the subroutine was invoked at every material integration point within the mesh. The upper/lower skin panel joints and the spar/skin panel joints were treated as permanently glued interfaces, thus component adhesive debonding was not considered. Also, the root joint fitting where the blade root connects to the hub was not explicitly modeled, where instead fixed boundary conditions were applied to the FE model in this region over a 1.0 m length.

Aerodynamic forces defined by Eqs. (2)–(3), and projected onto the FE model *X*- and *Y*-axes, as well as the centrifugal loads defined by Eq. (4), were applied through additional nodes defined at the blade segment aerodynamic centers (i.e., at the quarter-chord, mid-span locations) using automated ANSYS APDL algorithms. Each of these nodes were connected rigidly to the nodes on the corresponding blade segment skin panels, allowing for load distribution on each segment. Furthermore, the gravitational loading was applied as an acceleration body load to the entire meshed structure using the gravitational constant $g = 9.81$ m/s^2 (see Fig. 3).

3.3. Overall simulation procedure

Fig. 6 illustrates the overall simulation procedure for predicting damage evolution in wind turbine blade structures. Input data includes the blade geometry (NuMAD), FE mesh and boundary conditions, material properties and laminate stacking sequences, and structural loads. The loading sequence was controlled in the main simulation input file using ANSYS APDL programmable features, where for quasi-static conditions the aerodynamic, gravitational and centrifugal loads were incrementally increased up to the prespecified maximum, and the damage state was evaluated during each load step. For cyclic loading, the initial cycle ramp-up occurred under quasi-static conditions in order to determine the damage state after the first loading cycle, if any. After the first cycle ramp-down, all subsequent loading cycles involved explicit ramp-up and ramp-down segments where the evolving damage state was evaluated at the peak load. This explicit procedure is deemed suitable for structures loaded in the high cycle fatigue regime, where sub-critical damage evolution is prominent [8]. It should be noted that during the cyclic loading ramp-down segments, damage was assumed not to propagate since the structural stresses were decreasing and not fully reversible, which is similar to the procedure used in Ref. [47]. During the particular loading sequence, the subroutine was invoked for all material integration points during every single load step/cycle (see Fig. 6). ANSYS evaluated the structural displacements based on the current structural stiffness and passed the calculated strains to the subroutine, while the USERMAT evaluated the damage state and the stiffness and stress tensors which were passed back to ANSYS for the subsequent loading step. This process was repeated for every load step/cycle until a specified stopping criterion was met (i.e., maximum load or maximum cycle number).

4. Results and discussion

The developed multi-scale simulation model was used to predict sub-critical damage evolution in the wind turbine blade presented in Section 2, where two load cases were considered. First, the rotor blade was assumed to be in a parked position with the brake released when a sudden 15 m/s wind gust was imposed. This represents a critical operating condition, where a quasi-static simulation was performed. For the second load case, the blade was rotating constantly under a wind speed of 7.5 m/s when periodic wind gusts up to 11.25 m/s were imposed. This represents a normal operating condition [17], and was simulated as cyclic loading. Note that average wind speeds were used for both load cases, and

any commonly observed variations in wind speeds were not considered. Also, lower wind speeds were used in order to allow for evolution of sub-critical damage without the onset of structural damage modes or catastrophic failure.

4.1. Quasi-static loading

For the first load case, the reference two-spar rotor blade was chosen with a 2.8 m root chord, 5° twist angle, and $[0/90/\mp 45]_s$ GFRP laminate as the blade material. A plot of the tension-side skin panel axial stress along the blade length, between spar webs under the peak static load, is shown in Fig. 7a. Note that stress is zero near the root, which corresponds to the fixed 1.0 m region. A maximum stress of 550 MPa occurs at the location of the maximum root chord (i.e., 7.0 m), and the characteristic stress distribution near the root is due to the geometrical transition through this area (see Fig. 3). This variation of stress along the skin span is analogous to that reported by Bottasso et al. [11] for a 45 m long two-spar blade. The corresponding ply crack density variation is shown in Fig. 7b, where the peak crack density of 1.1 mm^{-1} corresponds to

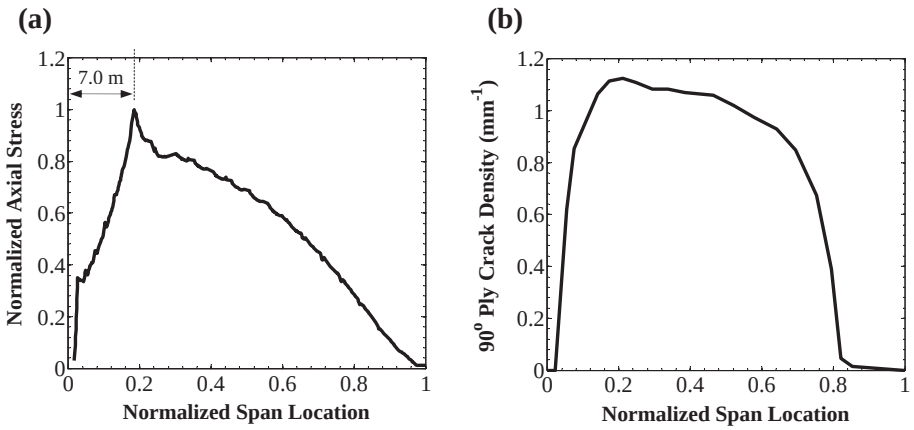

Fig. 7. Rotor blade with 2.8 root chord length, 5° twist angle and 15 m/s wind speed ramp-up: peak static load tension-side skin panel distribution (a) axial stress, (b) 90° ply crack density.

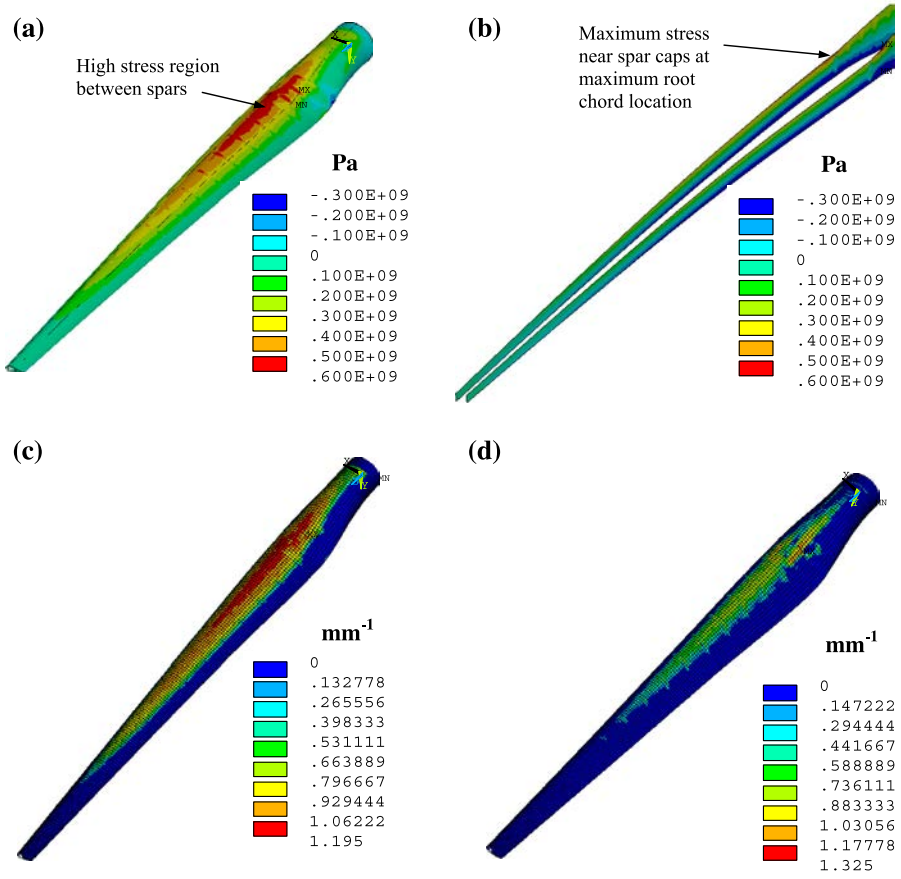

Fig. 8. Rotor blade with 2.8 root chord length, 5° twist angle and 15 m/s wind speed ramp-up: peak static load contours (a) tension-side skin panel axial stress, (b) spar web axial stress, (c) tension-side skin panel 90° ply crack density, tension-side skin panel 45° ply crack density.

the location of maximum axial stress, and the highly damaged region spans 65% of the blade length. Axial stress contours for the tension-side skin panel and spar webs are shown in Fig. 8a and b, while skin panel ply crack density contours for 90° and −45° plies are shown in Fig. 8c and d. The skin panel maximum stress and high crack density region is located between spar webs as is expected. Plots of crack density evolution for the skin panel at the maximum axial stress location are shown in Fig. 9a. The crack densities clearly plateau at these applied loads, which has been experimentally observed to signify the onset of delamination for multidirectional laminates [48,7], and also observed from full-scale test of wind turbine blades [3]. The study by Chen et al. [6] also reported that delamination of the skin panel and spar cap laminates in this region were the root cause of catastrophic blade failure. Thus, the developed model is able to predict the failure events preceding delamination and catastrophic failure. The evolving structural stiffness degradation is demonstrated by the blade tip flap-wise displacement evolution shown in Fig. 9b. It is clear from the plot that tip displacement is linear up to the point when ply cracking initiates, beyond which the tip deflection increases nonlinearly with a higher rate. This additional blade deflection of approximately 10% at the end of the simulation is

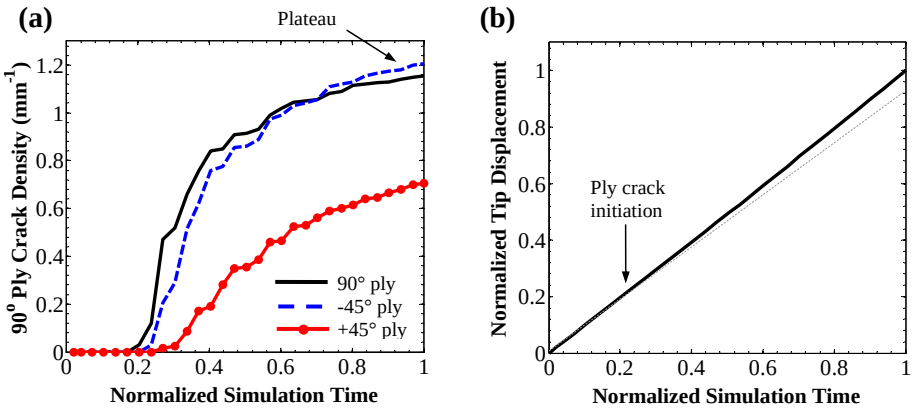

Fig. 9. Rotor blade with 2.8 root chord length, 5° twist angle and 15 m/s wind speed ramp-up (a) tension-side skin panel crack density evolution at maximum stress location, (b) blade tip flap-wise normalized displacement evolution.

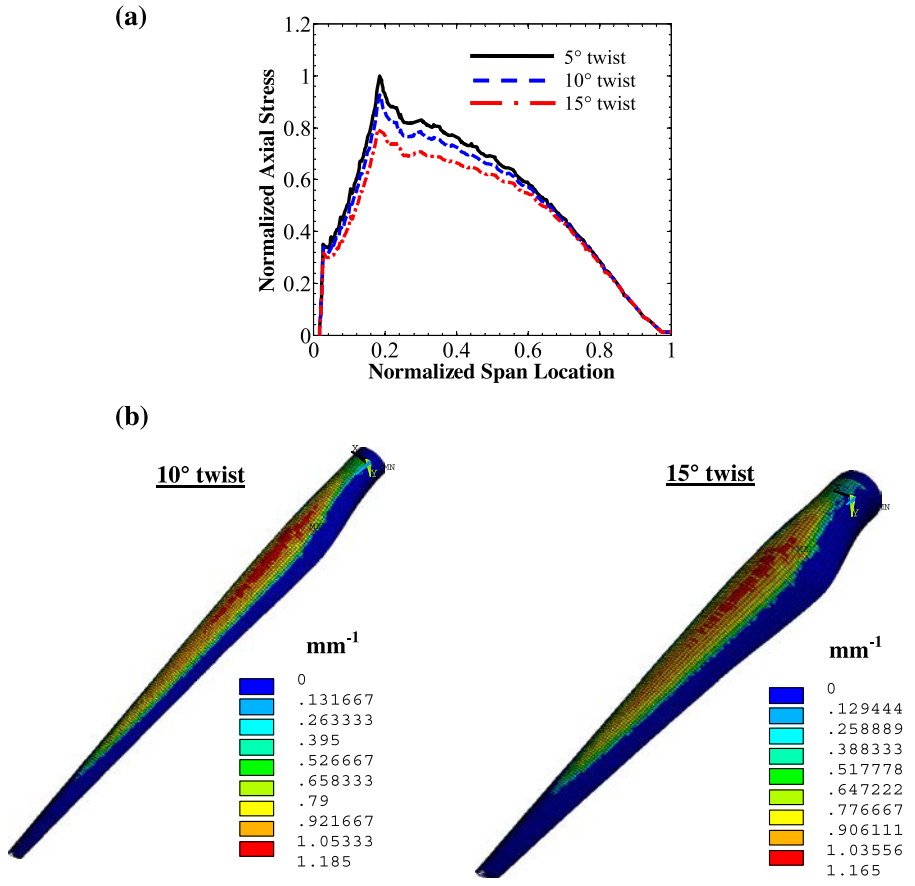

Fig. 10. Rotor blade with 2.8 root chord length, various twist angles, and 15 m/s wind speed ramp-up: peak static load (a) tension-side skin panel axial stress distributions, (b) 90° ply crack densities.

due to degradation of structural stiffness caused by ply crack multiplication in skin panels and spars.

4.2. Effect of twist angle and chord length on damage evolution

In order to demonstrate the effect of twist angle and root chord length on evolution of sub-critical damage, a parametric study was conducted for the reference rotor blade under quasi-static loading conditions. First, twist angles of 5°, 10° and 15° were considered, where a plot of the skin panel axial stress profile between the spar webs is shown in Fig. 10a. The peak axial stress, and the stress magnitude in the vicinity, notably decreases as twist angle increases. For example, when the twist angle increased from 5° to 15°, the maximum stress decreased by 20%. An increasing twist angle provides additional structural rigidity in the flap-wise bending direction, which tends to decrease the blade displacement and thus skin and spar stresses. This results in lower ply crack densities and a slightly reduced damage region (compare Figs. 8c and 10b). In the study by Tawade et al. [49] on wind turbine blades, it was found that fatigue life increased with increasing twist angle, which is in-line with the presented simulation results.

Next, maximum root chord lengths of 2.8 m, 3.8 m and 4.8 m were considered, while keeping the root diameter and tip chord length constant. The skin panel axial stress profile between the spar webs is shown in Fig. 11a, demonstrating that as the root chord length increases the peak axial stress magnitude decreases substantially (i.e., by 50% for the 4.8 m root chord length blade). This results from an increased blade width in this region, however, this comes at the cost of increased blade weight. Furthermore, it is also clear that the secondary stress peak close to the blade root increases in magnitude as the chord length increases (see Fig. 11a). This is a result of stress redistribution towards the root, caused by the greater blade geometric transition at larger chord lengths. This is an important point because a larger stress at the root may affect the root joint integrity. The corresponding ply crack density contours are shown in Fig. 11b, where the decrease in damage magnitude and a reduction in the size of the damage zone is shown (compare Figs. 8c and 11b). Also note the increased damage magnitude by 40% near the root as the chord length increases (see Fig. 11b).

4.3. Fatigue loading

Sub-critical damage contours at various cyclic intervals for a fatigue simulation of the reference two-spar rotor blade is shown in Fig. 12. After the first loading cycle the ply crack density of the 90° plies in the tension-side skin panel is localized between the spars, and in the spar webs, with peak value of 0.4 mm^{-1}. As the cyclic loading progresses the size of the damage zone expands along the length of the blade, as well as in the regions adjacent to the spars due to the localized stiffness degradation and resulting load redistribution, where by 1000 loading cycles the magnitude of the peak crack density in the 90° plies is 1.0 mm^{-1}. After 10,000 loading cycles, the magnitude of 90° ply crack density in the region between the spars has increased further, where the peak crack density reached a value near 1.1 mm^{-1}. Similar contour plots were predicted for cracking in the ±45° plies (not shown). Ply crack density evolution plots for the skin panel high stress region

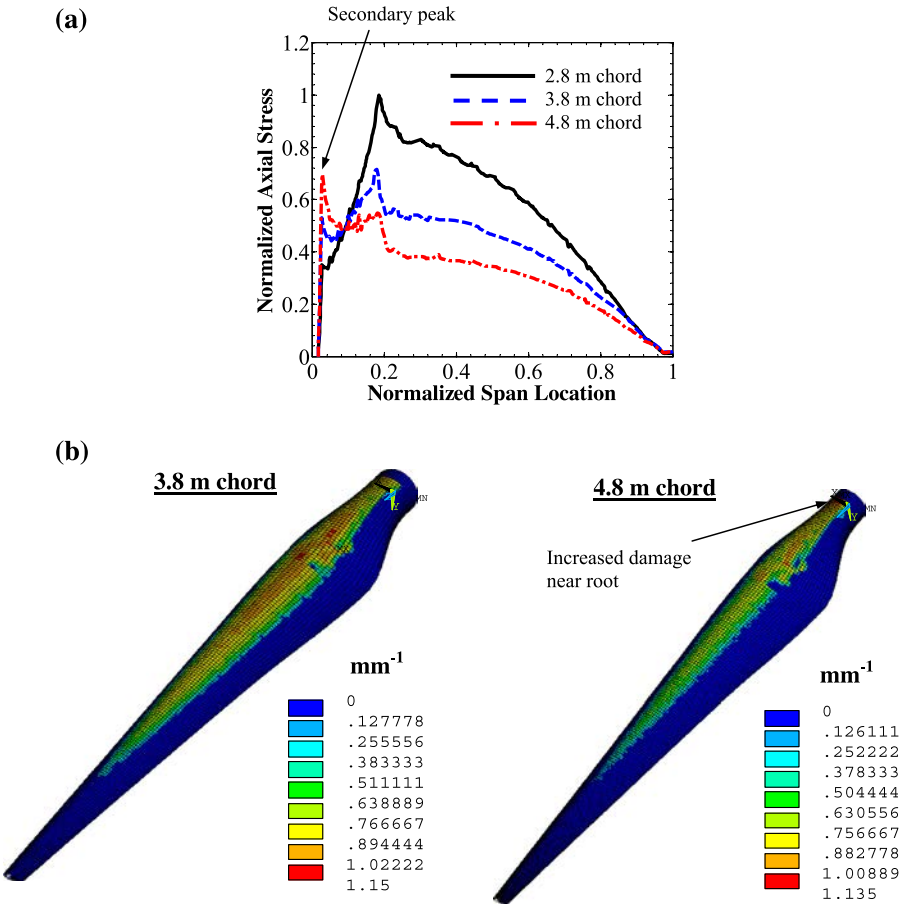

Fig. 11. Rotor blade with various root chord lengths, 5° twist angle, and 15 m/s wind speed ramp-up: peak static load (a) tension-side skin panel axial stress distributions, (b) 90° ply crack densities.

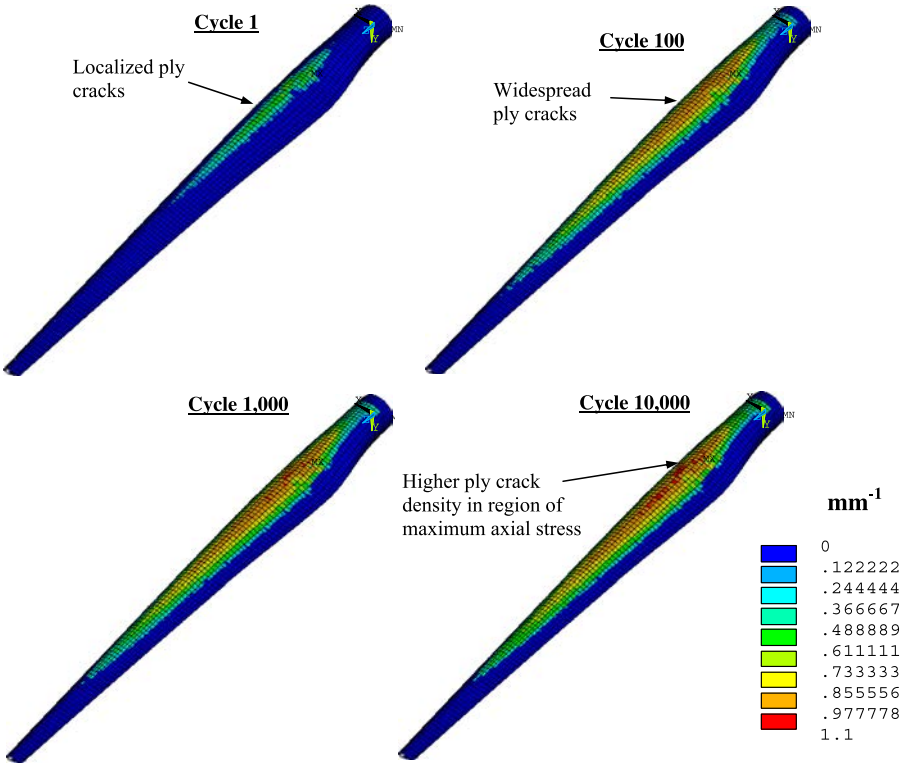

Fig. 12. 90° ply crack density contours for rotor blade skin panel with 2.8 root chord length, 5° twist angle and cycled between 7.5 m/s and 11.25 m/s wind speed.

between the spars are shown in Fig. 13a, revealing that these sub-critical cracks tend to saturate early on during loading for the considered wind speeds. Similar to the quasi-static simulations, the saturation of high density ply cracks in this region will eventually lead to localized delamination and skin/spar cap adhesive debonding, which was observed and reported by Sorensen et al. [3]. It should be noted that the onset of such critical damage modes does not imply that catastrophic blade failure will occur soon after, but will require additional load cycles. Nonetheless, the simulation results reveal that under the studied conditions the failure process begins during the early stages of cycling with sub-critical ply cracking, which is an important contribution for accurately predicting the damage tolerability of wind turbine structures. Finally, the blade tip flap-wise displacement evolution shown in Fig. 13b increases and plateau's during cyclic loading, which is analogous to the crack density plots, and is a direct result of the structural stiffness degradation caused by sub-critical damage evolution.

5. Conclusions

A multi-scale simulation model was developed for predicting sub-critical microscopic damage evolution and stiffness degradation in long composite wind turbine blade structures. The model included an integrated procedure for generating the blade geometry and the external loading (e.g., aerodynamic, gravitational, centrifugal), as well as an algorithm that simulated quasi-static and cycle-by-cycle fatigue loading. A developed user-defined

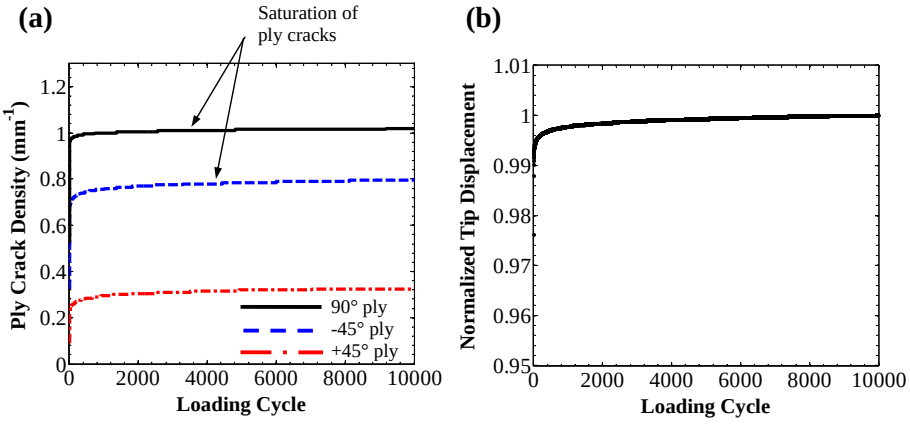

Fig. 13. Rotor blade with 2.8 root chord length, 5° twist angle and loaded cyclically (a) tension-side skin panel crack density evolution at maximum stress location, (b) evolution of blade tip flap-wise normalized displacement.

subroutine combining computational micromechanics and continuum damage mechanics was implemented into a commercial finite element software package, which was also utilized by the simulation model. The developed multi-scale model does not require extensive and costly experimental test data for calibration of the damage parameters, which can be considered as an improvement over previous approaches. The simulation results for both quasi-static and fatigue loading cases clearly demonstrated the ability of the model to predict the evolution of sub-critical ply cracks in the critical regions of the blade structure, i.e., on the spar structure and the skin panels near the spar caps. This is an important contribution since the developed model accounts for the early stages of progressive structural failure, which is vital for increasing the accuracy of damage tolerance analysis of structures and for structural health monitoring. In addition, a parametric study revealed that the blade twist angle and root chord length directly influenced the evolution of sub-critical damage, where an increase in the root chord length from 2.8 m to 3.8 m decreased the size and magnitude of the damage zone by 30%. This is important for optimization of blade designs, and provides valuable insight for potentially delaying the onset of critical damage modes in wind turbine blade structures.

In order to certify wind turbine structures, it is necessary to predict the multi-scale nature of damage evolution in rotor blades (i.e., sub-critical ply cracking, followed by delamination and adhesive debonding, and finally catastrophic failure). The developed model predicts sub-critical damage evolution up to the onset of critical damage, however, ongoing work is aimed at expanding the simulation model in order to simulate critical damage modes and ultimately structural collapse. First, the model will be expanded to include cohesive elements in order to predict structural debonding at the spar/skin panel and upper/lower skin panel joints, and at the skin/root joint fitting interface. In addition, various laminates will be used to model the blade geometry in lieu of the assumed constant laminate material, where ply transitions will be accounted for. Structural buckling caused by compressive loads, and the associated delamination, will also be included in the simulation model. Finally, based on reported wind speed data realistic loading spectra will also be incorporated in lieu of approximated constant wind speeds.

Acknowledgements

The authors thank the Natural Sciences and Engineering Research Council of Canada (NSERC), and the University of Toronto for funding in support of this work. We would also like to express our gratitude to ANSYS and SimuTech for their support throughout this project.

References

[1] Sorensen BF. Materials and structures for wind turbine rotor blades – an overview. In: Proceedings of the 17th international conference on composite materials (ICCM 17), Edinburgh; 27–31 July 2009.
[2] Talreja R. Multi-scale modeling in damage mechanics of composites. J Mater Sci 2006;41:6800–12.
[3] Sorensen BF, Jorgensen E, Debel CP, Jensen FM, Jensen HM, Jacobsen TK, Halling KM. Improved design of large wind turbine blade of fibre composites based on studies of scale effects (Phase 1). RISO National Laboratory Report (RISO-R-1390), Denmark; September 2004.
[4] Overgaard LCT, Lund E, Camanho PP. A methodology for the structural analysis of composite wind turbine blades under geometric and material induced instabilities. Compos Struct 2010;88:1092–109.
[5] Yang J, Peng C, Xiao J, Zeng J, Xing S, Jin J, et al. Structural investigation of composite wind turbine blade considering structural collapse in full-scale static tests. Compos Struct 2013;97:15–29.
[6] Chen X, Zhao W, Zhao XL, Xu JZ. Preliminary failure investigation of a 52.3 m glass/epoxy composite wind turbine blade. Eng Fail Anal 2014;44:345–50.
[7] Lambert J, Chambers AR, Sinclair I, Spearing SM. 3D damage characterisation and the role of voids in the fatigue of wind turbine blade materials. Compos Sci Technol 2012;72:337–43.
[8] Hosseini-Toudeshky H, Jahanmardi M, Goodarzi MS. Progressive debonding analysis of composite blade root joint of wind turbines under fatigue loading. Compos Struct 2015;120:417–27.
[9] Hayat K, Ha SK. Load mitigation of wind turbine blade by aeroelastic tailoring via unbalanced laminate composites. Compos Struct 2015;128:122–33.
[10] Pollayi H, Yu W. Modeling matrix cracking in composite rotor blades within VABS framework. Compos Struct 2014;110:62–76.
[11] Bottasso CL, Campagnolo F, Croce A, Dilli A, Gualdoni F, Nielsen MB. Structural optimization of wind turbine rotor blades by multilevel sectional/multibody/3D-FEM analysis. Multibody Syst Dyn 2014;32:87–116.
[12] Cardenas D, Elizalde H, Marzocca P, Gallegos S, Probst O. A couples aeroelastic damage progression model for wind turbine blades. Compos Struct 2012;94:3072–81.
[13] Leong M, Overgaard LCT, Thomsen OT, Lund E, Daniel IM. Investigation of failure mechanisms in GFRP sandwich structures with face sheet wrinkle defects used for wind turbine blades. Compos Struct 2012;94:768–78.
[14] Abumeri G, Abdi F. Advanced composite wind turbine blade design based on durability and damage tolerance. AlphaSTAR Corporation Report (ASC-2011-DOE-1), US; November 2011.
[15] Duan W, Zhao F. Loading analysis and strength calculation of wind turbine blade based on blade element momentum theory and finite element method. In: Proceedings of the power and energy engineering conference (APPECC) – IEEE, Chengdu; 28–31 March 2010.
[16] Rajadurai JS, Thanigaiyarasu G. Failure envelope generation using modified failure criteria for wind turbine blade and validation for FRP laminates. Mech Adv Mater Struct 2009;16:275–92.
[17] Shokrieh MM, Rafiee R. Simulation of fatigue failure in a full composite wind turbine blade. Compos Struct 2006;74:332–42.
[18] Kensche CW. Fatigue of composites for wind turbines. Int J Fatigue 2006;28:1363–74.
[19] Talreja R. Assessment of the fundamentals of failure theories for composite materials. Compos Sci Technol 2014;105:190–201.
[20] Bogdanor MJ, Oskay C, Clay SB. Multiscale modeling of failure in composites under model parameter uncertainty. Comput Mech 2015;56:389–404.
[21] Crouch RD, Clay SB, Oskay C. Experimental and computational investigation of progressive damage accumulation in CFRP composites. Compos Part B 2013;48:59–67.
[22] Maimi P, Camanho PP, Mayugo JA, Davila CG. A continuum damage model for composite laminates: part I – constitutive model. Mech Mater 2007;39:897–908.
[23] Maimi P, Camanho PP, Mayugo JA, Davila CG. A continuum damage model for composite laminates: part II – computational implementation and validation. Mech Mater 2007;39:909–19.
[24] Lopes CS, Sadaba S, Gonzalez C, Llorca J, Camanho PP. Physically-sound simulation of low-velocity impact on fiber reinforced laminates. Int J Impact Eng 2015. http://dx.doi.org/10.1016/j.ijimpeng.2015.05.014.
[25] Pineda EJ, Waas AM, Bednarcyk BA, Collier CS. Multiscale model for progressive damage and failure of laminated composites using an explicit finite element method. In: Proceedings of the 50th AIAA/ASME/ASCE/AHS/ASC structures, structural dynamics, and materials conference, Palm Springs; 4–7 May 2009.
[26] Pineda EJ, Waas AM. Numerical implementation of a multiple-ISV thermodynamically-based work potential theory for modeling progressive damage and failure in fiber-reinforced laminates. Int J Fract 2013;182:93–122.
[27] Hallett SR, Green BG, Jiang WG, Wisnom MR. An experimental and numerical investigation into the damage mechanisms in notched composites. Compos Part A 2009;40:613–24.
[28] Xu X, Wisnom MR, Li X, Hallett SR. A numerical investigation into size effects in centre-notched quasi-isotropic carbon/epoxy laminates. Compos Sci Technol 2015;111:32–9.
[29] Montesano J, Singh CV. A synergistic damage mechanics based multiscale model for composite laminates subjected to multiaxial strains. Mech Mater 2015;83:72–89.
[30] Montesano J, Singh CV. Predicting evolution of ply cracks in composite laminates subjected to biaxial loading. Compos Part B 2015;75:264–73.
[31] Laird DL. Numerical manufacturing and design tool (NuMAD) user manual. Report no. SAND2001-2375. Wind energy technology. Sandia National Laboratories; 2001.
[32] Somers DM. The S816, S817, and S818 airfoils. National renewable energy laboratory report (NREL/SR-500-36333). US Department of Energy; December 2004.
[33] Schubel PJ, Crossley RJ. Wind turbine blade design. Energies 2012;5:3425–49.
[34] Hao E. Wind turbines, fundamentals, technologies, application, economics. 2nd ed. Berlin: Springer; 2006.
[35] Davalos JF, Qiao P, Wang J, Salim HA, Schlussel J. Shear moduli of structural composites from torsion tests. J Compos Mater 2002;36:1151–73.
[36] Tong J, Guild FJ, Ogin SL, Smith PA. On matrix crack growth in quasi-isotropic laminates – I. Experimental investigation. Compos Sci Technol 1997;57:1527–35.
[37] Varna J, Joffe R, Akshantala VN, Talreja R. Damage in composite laminates with off-axis plies. Compos Sci Technol 1999;59:2139–47.
[38] Kashtalyan M, Soutis C. Stiffness and fracture analysis of laminated composites with off-axis ply matrix cracking. Compos Part A 2007;38:1262–9.
[39] Talreja R. Damage characterization by internal variables. In: Talreja R, editor. Damage mechanics of composite materials. Amsterdam: Elsevier; 1994. p. 53–78.

[40] Li S, Singh CV, Talreja R. A representative volume element based on translational symmetries for FE analysis of cracked laminates with two arrays of cracks. Int J Solids Struct 2009;46:1793–804.
[41] Joffe R, Krasnikovs A, Varna J. COD-based simulation of transverse cracking and stiffness degradation reduction in $[S/90_n]_s$ laminates. Compos Sci Technol 2001;61:637–56.
[42] Singh CV, Talreja R. Evolution of ply cracks in multidirectional composite laminates. Int J Solids Struct 2010;47:1338–49.
[43] Bazant ZP, Le JL, Bazant Z. Scaling of strength and lifetime probability distributions of quasibrittle structures based on atomistic fracture mechanics. Proc Nat Acad Sci 2009;106:11484–9.
[44] Le JL, Bazant ZP, Bazant MZ. Unified nano-mechanics based probabilistic theory of quasibrittle and brittle structures: I. strength, static crack growth, lifetime and scaling. J Mech Phys Solids 2011;59:1291–321.
[45] Highsmith AL, Reifsnider KL. Stiffness-reduction mechanisms in composite laminates. In: Reifsnider KL, editor. Damage in composite materials. Philadelphia: ASTM STP 775; 1982. p. 103–17.
[46] ANSYS v15.0 user manual. ANSYS Inc.: Cannonsburg, PA; 2011.
[47] Montesano J, Selezneva M, Levesque M, Fawaz Z. Modeling fatigue damage evolution in polymer matrix composite structures and validation using in-situ digital image correlation. Compos Struct 2015;125:354–61.
[48] Masters JE, Reifsnider KL. An investigation of cumulative damage development in quasi-isotropic graphite/epoxy laminates. In: Reifsnider KL, editor. Damage in composite materials. Philadelphia: ASTM STP 775; 1982. p. 40–62.
[49] Tawade SV, Todkar SB, Hade AS. Fatigue life optimization of wind turbine blade. Int J Res Eng Technol 2014;3:843–50.